Bifurcations in a Mathieu equation with cubic nonlinearities: Part II ☆

Leslie Ng *, Richard Rand

Department of Theoretical and Applied Mechanics, Cornell University, Ithaca, NY 14853, USA

Abstract

In a previous paper [Chaos Solitons Fract. 14(2) (2002) 173], the authors investigated the dynamics of the equation:

$$\frac{\mathrm{d}^2x}{\mathrm{d}t^2} + (\delta + \epsilon\cos t)x + \epsilon\left[Ax^3 + Bx^2\left(\frac{\mathrm{d}x}{\mathrm{d}t}\right) + C x\left(\frac{\mathrm{d}x}{\mathrm{d}t}\right)^2 + D\left(\frac{\mathrm{d}x}{\mathrm{d}t}\right)^3\right] = 0$$

We used the method of averaging in the neighborhood of the 2:1 resonance in the limit of small forcing and small nonlinearity. We found that a degenerate bifurcation point occurs in the resulting slow flow and some of the bifurcations near this point were looked at. In this work we present additional results concerning the bifurcations around this point using analytic techniques and AUTO. An analytic approximation for a heteroclinic bifurcation curve is obtained. Additional results on the bifurcations of periodic orbits in the slow flow are also presented.
© 2002 Published by Elsevier Science B.V.

☆ Part I of this research was published in Chaos, Solitons and Fractals 2002; 14(2) 173–81.
* Corresponding author.
E-mail address: lhn2@cornell.edu (L. Ng).

1. Introduction

In a previous paper [6], we looked at the following equation:

$$\frac{d^2x}{dt^2} + (\delta + \epsilon \cos t)x + \epsilon\left[Ax^3 + Bx^2\left(\frac{dx}{dt}\right) + Cx\left(\frac{dx}{dt}\right)^2 + D\left(\frac{dx}{dt}\right)^3\right] = 0 \tag{1}$$

Omitting nonlinear terms in Eq. (1) results in the linear Mathieu equation which frequently arises in physics and engineering. The additional x^3 term may come from a nonlinear stiffness (e.g. the vertically forced pendulum). The $(dx/dt)^3$ term could come from nonlinear damping (e.g., a model of high speed drag). The $x^2(dx/dt)$ term is a nonlinear position-dependent damping like the term in the Van der Pol equation. The $x(dx/dt)^2$ term may come from a nonlinear inertia term (e.g. in systems where the kinetic energy $T = \frac{1}{2}mx^2(dx/dt)^2$).

Some other recent studies involving nonlinear Mathieu equations are as follows: Norris [5] studied the bifurcations in a Mathieu equation with x^2 and x^3 terms. Kidachi and Onogi [4] looked at the stability of a Mathieu equation with only the x^3 term. El-Dib [2] analyzed an equation of the form:

$$\frac{d^2x}{dt^2} + (a_1 - 2\epsilon q_1 \cos 2t)x + (a_2 - 2\epsilon q_2 \cos 4t)x^2 + (a_3 - 2\epsilon q_3 \cos 6t)x^3 = 0 \tag{2}$$

To detune off the 2:1 resonance we set:

$$\delta = \frac{1}{4} + \delta_1 \epsilon \tag{3}$$

Applying the method of averaging to first-order gives the following slow flow:

$$\frac{dR}{dt} = \epsilon\left(\frac{R}{2}\sin 2\psi - \beta R^3\right) \tag{4}$$

$$\frac{d\psi}{dt} = \epsilon\left(\delta_1 + \frac{1}{2}\cos 2\psi + \alpha R^2\right) \tag{5}$$

where

$$\alpha = \frac{3}{4}A + \frac{1}{16}C \quad \text{and} \quad \beta = \frac{1}{8}B + \frac{3}{32}D \tag{6}$$

and where

$$x \approx R\cos\left(\frac{t}{2} + \psi\right), \quad \dot{x} \approx -\frac{R}{2}\sin\left(\frac{t}{2} + \psi\right) \tag{7}$$

To explain some of the features observed by numerically integrating the system, we found that it was necessary to go to second-order in the averaging procedure [9,10]. To make the problem more tractable, we arbitrarily fixed the parameters:

$$A = 1, \quad B = 3 \tag{8}$$

and we scaled:

$$\alpha = \beta = \epsilon\mu \tag{9}$$
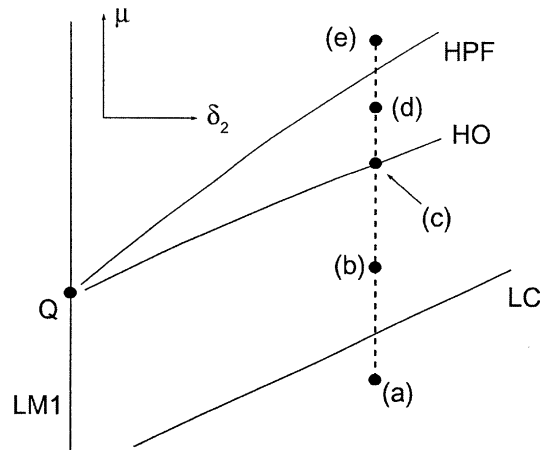
Fig. 1. Bifurcations near point Q ($\delta_1 = -1/2$, $\delta_2 = -1/8$ and $\mu = 0$). Phase portraits along path (dashed line) shown in Fig. 2.

We also expanded δ to $O(\epsilon^2)$ terms:

$$\delta = \frac{1}{4} + \delta_1\epsilon + \delta_2\epsilon^2 \tag{10}$$

Substituting Eqs. (8)–(10) into Eq. (1) and applying the method of averaging to second-order results in the simplified slow flow equations:

$$\frac{dR}{dt} = \epsilon\left[\frac{1}{2}R\sin 2\psi\right] + \epsilon^2\left[-\delta_1 R\sin 2\psi + \left(\frac{3}{2}\delta_1 - \mu + \frac{1}{2}\sin 2\psi + \frac{1}{4}\cos 2\psi\right)R^3\right] \tag{11}$$

$$\frac{d\psi}{dt} = \epsilon\left[\delta_1 + \frac{1}{2}\cos 2\psi\right] + \epsilon^2\left[\delta_2 - \delta_1^2 - \frac{1}{8} - \delta_1\cos 2\psi + (\mu - 3\delta_1 + \sin 2\psi - 2\cos 2\psi)R^2 - \frac{15}{8}R^4\right] \tag{12}$$

A combination of analytic and numerical techniques were used to analyze the simplified slow flow equations. The AUTO bifurcation and continuation software [1] was used to numerically generate bifurcation diagrams. A degenerate bifurcation point Q was found to occur for the parameter values $\delta_1 = -1/2$, $\delta_2 = -1/8$ and $\mu = 0$. Fig. 1 illustrates the bifurcations near point Q and Fig. 2 shows the corresponding phase portraits for the path in parameter space shown in Fig. 1 from (a) to (e).

In Fig. 1, bifurcations occur along the solid curves. The left transition curve of the 2:1 resonance in the linear Mathieu equation corresponds to LM1 where a bifurcation of fixed points on $R = 0$ occurs in the slow flow. In our previous paper, we refer to *type 1* periodic orbits as those which plot as a topological circle in the $R - \psi$ phase space (see Fig. 2d) and to *type 2* periodic orbits as those which are topologically equivalent to $R = \text{const}$ (see Fig. 2b). On the curve labelled LC, a type 2 limit cycle is created at ∞. An analytic expression for the LC curve was obtained in the previous paper. HPF corresponds to a curve of Hopf bifurcations where a type 1 periodic orbit is created. HO denotes a curve of heteroclinic bifurcations where a periodic orbit changes from type 1 to type 2. It appears that the HO and HPF curves meet at a common point Q on the LM1 curve.
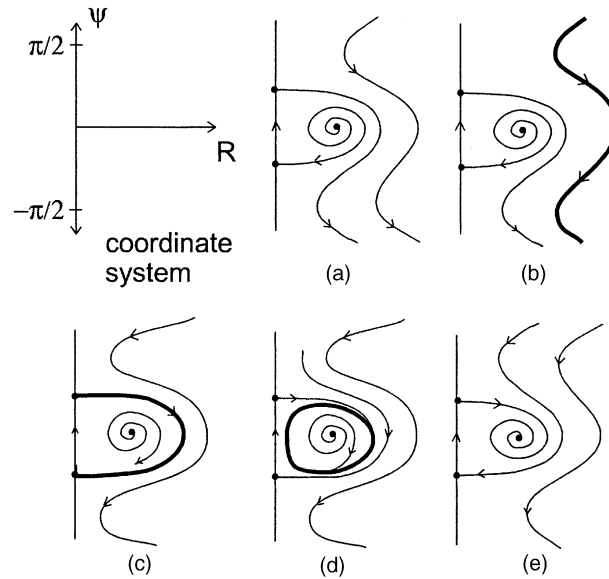
Fig. 2. Phase portraits corresponding to Fig. 1. Darker line corresponds to a stable periodic orbit.

In this paper, we are interested in the behavior of Eqs. (11) and (12) in the neighborhood of the bifurcation point Q. We shall see that although Fig. 1 is correct, it is incomplete, in the sense that there is a lot of detail (in the form of additional bifurcations) occurring near point Q which is omitted from Fig. 1. Since we are interested in the neighborhood of point Q, for which $\delta_1 = -1/2$, $\delta_2 = -1/8$ and $\mu = 0$, we will set $\delta_1 = -1/2$ in Eqs. (11) and (12) throughout this paper, which gives:

$$\frac{\mathrm{d}R}{\mathrm{d}t} = \epsilon \left[\frac{1}{2} R \sin 2\psi \right] + \epsilon^2 \left[\frac{1}{2} R \sin 2\psi + \left(-\frac{3}{4} - \mu + \frac{1}{2} \sin 2\psi + \frac{1}{4} \cos 2\psi \right) R^3 \right] \tag{13}$$

$$\frac{\mathrm{d}\psi}{\mathrm{d}t} = \epsilon \left[-\frac{1}{2} + \frac{1}{2} \cos 2\psi \right] + \epsilon^2 \left[\delta_2 - \frac{3}{8} + \frac{1}{2} \cos 2\psi + \left(\mu + \frac{3}{2} + \sin 2\psi - 2 \cos 2\psi \right) R^2 - \frac{15}{8} R^4 \right] \tag{14}$$

For these equations, we will take μ and δ_2 as unfolding parameters and we will consider ϵ to be small but fixed.

2. Analytic results obtained in part I [6]

To investigate the bifurcations near point Q, an unfolding around Q was performed [6]. We began by using the rescaling:

$$R = \sigma \sqrt{u}, \quad \psi = \sigma v, \quad \mu = \sigma v_1, \quad \delta_2 = -1/8 + \sigma^2 v_2, \quad \tau = \epsilon \sigma t, \quad \text{for } \sigma \text{ small} \tag{15}$$

The rescaling was chosen so that when $\sigma = 0$, the system is Hamiltonian with a heteroclinic connection (which will be needed in a later calculation). Substituting Eq. (15) into Eqs. (13) and (14) and Taylor expanding in σ gives:

$$\frac{du}{d\tau} = 2(1+\epsilon)uv - \epsilon u^2\sigma - \left[2(v_1 - v)\epsilon u^2 + \frac{4}{3}(1+\epsilon)uv^3\right]\sigma^2 - \epsilon u^2 v^2\sigma^3 + O(\sigma^4) \tag{16}$$

$$\frac{dv}{d\tau} = v_2\epsilon - (1+\epsilon)v^2 - \frac{\epsilon}{2}u + (v_1 + 2v)\epsilon u\sigma + \left[4\epsilon uv^2 - \frac{15}{8}\epsilon u^2 + \frac{1}{3}(1+\epsilon)v^4\right]\sigma^2 - \frac{4}{3}\epsilon uv^3\sigma^3 + O(\sigma^4) \tag{17}$$

In our previous analysis of the unfolding, we obtained the following approximation of the Hopf bifurcation curve HPF emanating out of point Q [6]:

$$\mu = \frac{3\epsilon(\delta_2 + 1/8)}{1+\epsilon} + \frac{9\epsilon(11\epsilon + 5)(\delta_2 + 1/8)^2}{2(1+\epsilon)^2} + \cdots \tag{18}$$

3. Analytic approximation of heteroclinic bifurcation

Although the approximation (18) for the Hopf bifurcation curve HPF was found in our previous work [6], we did not have an analytic approximation for the heteroclinic bifurcation curve HO. In this section, we will derive such an approximation. We begin by assuming a series expansion for u of the form:

$$u(v) = u_0(v) + u_1(v)\sigma + u_2(v)\sigma^2 + u_3(v)\sigma^3 + \cdots \tag{19}$$

We then divide Eq. (16) by Eq. (17) and substitute in Eq. (19). Taylor expanding in σ, we get:

$$\frac{du_0}{dv} + \frac{du_1}{dv}\sigma + \frac{du_2}{dv}\sigma^2 + \frac{du_3}{dv}\sigma^3 + \cdots = F_0(u_0, v) + F_1(u_0, u_1, v)\sigma + F_2(u_0, u_1, u_2, v)\sigma^2$$
$$+ F_3(u_0, u_1, u_2, u_3, v)\sigma^3 + \cdots \tag{20}$$

Equating like powers of σ, we get a series of first-order ODE's for u_i:

$$O(1): \quad \frac{du_0}{dv} = F_0(u_0, v) = -\frac{4(1+\epsilon)u_0 v}{2(1+\epsilon)v^2 + \epsilon u_0 - 2\epsilon v_2} \tag{21}$$

$$O(\sigma): \quad \frac{du_1}{dv} = F_1(u_0, u_1, v) = \frac{N_1(u_0, u_1, v)}{D_1(u_0, u_1, v)} \tag{22}$$

$$O(\sigma^2): \quad \frac{du_2}{dv} = F_2(u_0, u_1, u_2, v) = \frac{N_2(u_0, u_1, u_2, v)}{D_2(u_0, u_1, u_2, v)} \tag{23}$$

$$O(\sigma^3): \quad \frac{du_3}{dv} = F_3(u_0, u_1, u_2, u_3, v) = \frac{N_3(u_0, u_1, u_2, u_3, v)}{D_3(u_0, u_1, u_2, u_3, v)} \tag{24}$$

where the functions N_i and D_i are too long to be given here.

We can solve for $u_0(v)$ from the O(1) ODE (21) and then substitute the solution into the O(σ) ODE (22) for $u_1(v)$ where $F_1(u_0, u_1, v)$ becomes only a function of u_1 and v which we can now solve. Similarly, we can substitute our solution for $u_1(v)$ into the ODE (23) for $u_2(v)$ and so on. The constants of integration C_i that we get when solving each ODE for the u_i are determined by requiring the solution go through the two fixed points of the heteroclinic orbit.

In applying this procedure, we start by finding a series approximation for the two fixed points on the heteroclinic orbit. We know that these points occur at $u^* = 0$ and finding a series solution for v^* is straight-forward using regular perturbations. The series approximations for the two fixed points on the heteroclinic orbit (denoted by $+$ and $-$) are

$$u_{\pm}^* = 0, \quad v_{\pm}^* = \pm\sqrt{\frac{\epsilon v_2}{\epsilon+1}} \pm \frac{\sigma^2\epsilon^2 v_2^2}{6(\epsilon+1)^2}\sqrt{\frac{\epsilon+1}{\epsilon v_2}} + O(\sigma^4) \tag{25}$$

Now to solve for the constants C_i obtained from solving each ODE, we require that our series expansion for $u(v)$ goes through the fixed points $u_{\pm}^*$, $v_{\pm}^*$ (valid up to order $O(\sigma^i)$). When solving the O(1) ODE (21), a value for C_0 can be chosen so that the solution goes through both fixed points. The solution of $u_0(v)$ corresponds to the Hamiltonian case which are perturbing off so this is expected. We find that this is also the case for C_1 when solving the $O(\sigma)$ ODE (22). When solving the $O(\sigma^2)$ and $O(\sigma^3)$ ODE's, C_2 and C_3 can no longer be chosen so the solution $u(v)$ goes through both fixed points for all parameter values. At this order in σ, the heteroclinic orbit only exists for specific parameter values (at the heteroclinic bifurcation). We choose values for C_2 and C_3 so $u(v)$ goes through only one of the two fixed points. For $u(v)$ to go through the other of the two fixed points, we obtain a condition on the parameters of the system for the heteroclinic orbit to exist.

The result of this calculation is the following equation for the heteroclinic bifurcation curve HO (see [7] for details):

$$\mu = \frac{45\epsilon(\delta_2 + 1/8)}{14(1+\epsilon)} - \frac{16095\epsilon^2(\delta_2 + 1/8)^2}{392(1+\epsilon)^2} + \cdots \tag{26}$$

4. Crossing of Hopf and heteroclinic bifurcation curves

From Fig. 1, we see that the HPF bifurcation curve lies above the HO bifurcation curve away from the point Q ($\delta_1 = -1/2$, $\delta_2 = -1/8$, $\mu = 0$) in the $\delta_2 - \mu$ parameter plane. However, using the analytic approximations we have obtained, valid in the neighborhood of point Q, we find that the opposite is true! The first term of the HPF approximation (Eq. (18)) is

$$\mu = \frac{3\epsilon(\delta_2 + 1/8)}{1+\epsilon} + \cdots \tag{27}$$

The first term of the HO approximation (Eq. (26)) is

$$\mu = \frac{45\epsilon(\delta_2 + 1/8)}{14(1+\epsilon)} + \cdots \tag{28}$$

Comparing Eqs. (27) and (28), it is clear that the HO curve comes out of point Q with a steeper slope that the HPF curve. It turns out that the HO curves lies above the HPF curve only in a very small region near point Q. As we get farther away from point Q, the two curves eventually intersect after which the HO curve lies below the HPF curve and we are back to the situation outlined in Fig. 2. We use AUTO to verify this. Fig. 3 shows the HO and HPF curves obtained using AUTO near the degenerate bifurcation point Q. Here, we hold $\epsilon = 0.01$ fixed and varying δ_2 and μ since we are concerned with the behavior close the degenerate bifurcation point.
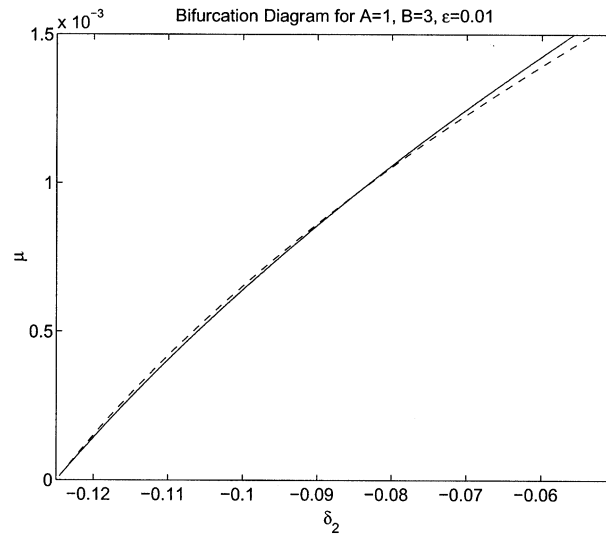
Fig. 3. HPF and HO curves for $A = 1$, $B = 3$, $\epsilon = 0.01$, $\alpha = \beta = \epsilon\mu$ obtained by using AUTO for Eqs. (13) and (14) near the degenerate bifurcation point Q ($\mu = 0$, $\delta_2 = -\frac{1}{8}$). Solid line is HPF curve, dashed line is HO curve.

5. Bifurcation diagram about point Q

We now present a complete picture of the bifurcations that occur near the degenerate bifurcation point Q. We first summarize our results. Fig. 4 shows the bifurcation diagram near point Q (see Table 1) and Fig. 5 shows the phase portraits corresponding to different regions in Fig. 4. Note that in Fig. 4 the features have been exaggerated to make them more visible.

We find that there are three additional bifurcation curves involving the bifurcation of periodic orbits: SPO1 which corresponds to a saddle-node bifurcation of type 1 periodic orbits, SPO2
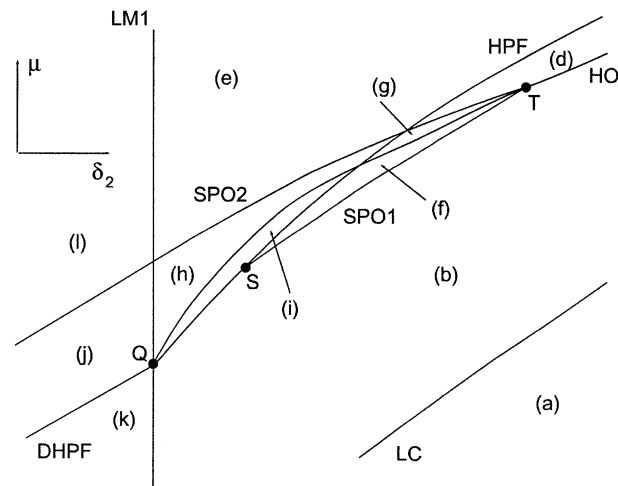
Fig. 4. Bifurcation diagram for $A = 1$, $B = 3$, $\delta_1 = -1/2$ near point Q. Regions denoted by lower case letters in ( ) have corresponding phase portraits shown in Fig. 5. See Table 1.

Table 1
Labels for bifurcation curves used in Fig. 4

Label	Curve
LM1	Transition curve of linear Mathieu equation
LC	Limit cycle created at ∞
HO	Heteroclinic bifurcation
HPF	Hopf bifurcation
SPO1	Saddle-node of type 1 period orbits
SPO2	Saddle-node of type 2 period orbits
DHPF	Degenerate Hopf bifurcation
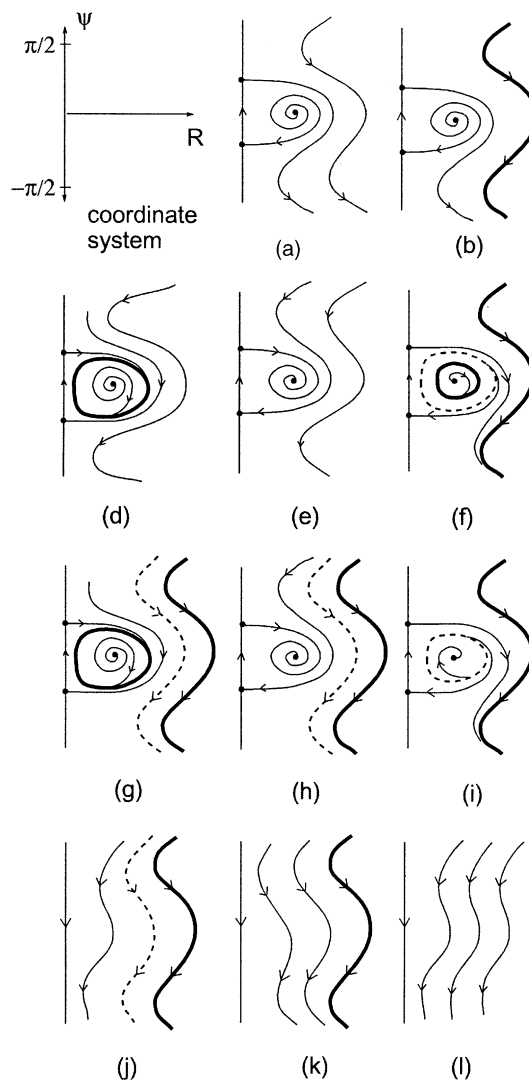
Fig. 5. Phase portraits for different regions near point Q (see Fig. 4). Darker lines correspond to stable periodic orbits. Dashed lines correspond to unstable periodic orbits.

which corresponds to a saddle-node bifurcation of type 2 periodic orbits and a curve of degenerate Hopf bifurcations DHPF which corresponds to a type 2 periodic orbit emerging from $R = 0$ (to be discussed in a following section). The point S denotes where the SPO1 curve appears to emanate from the HPF curve and the point T denotes a point on the HO curve where the both SPO1 and SPO2 curves appear to come out from. AUTO was again used to obtain numerical data for these new bifurcation curves.

6. Approximation of saddle-node bifurcation of periodic orbits and degenerate Hopf bifurcation curves using AUTO

To obtain an approximation for the SPO1 curve, we use AUTO to continue periodic orbits from points on the Hopf bifurcation curve HPF. Holding δ_2 fixed, we continue in μ from points on the HPF curve near the intersection of the HO and HPF curves where we expect to find the SPO1 curve. When we start the continuation, μ initially decreases because we have chosen to continue from a point on the HPF curve where the periodic orbits grow out of the equilibrium point as μ decreases. At some point AUTO will detect a fold and μ starts to increase. This corresponds to a point on the SPO1 curve. If we continue after the fold, we will eventually reach the HO curve in a heteroclinic bifurcation. This procedure can be repeated for different starting points on the HPF curve to obtain the SPO1 curve. Fig. 6 shows an illustration of this procedure. Fig. 7 shows the SPO1 curve obtained along with the HO and HPF curves in a region zoomed in around where the HO and HPF curves cross.

To investigate the SPO2 and DHPF curves, it is more convenient to look at the slow flow equations around point Q, Eqs. (13) and (14), if we transform to cartesian coordinates. We do this for the following reasons:

(1) The resulting equations are polynomial equations and do not contain trigonometric terms which are more difficult to deal with computationally.
(2) The origin $x = 0$, $\dot{x} = 0$ in the original equation is singular in polar coordinates (for $R = 0$, ψ is undefined). This is not the case in cartesian coordinates where the origin in the original equation is now $w = 0$, $z = 0$. In cartesian coordinates, the type 1 periodic orbits encircle non-origin equilibria and the type 2 periodic orbits encircle the origin. Also, the bifurcation we refer to as a heteroclinic bifurcation in polar coordinates is a homoclinic bifurcation with two loops in cartesian coordinates. Fig. 8 shows some phase portraits in both polar $R - \psi$ and cartesian $w - z$ coordinates.

To transform to cartesian coordinates we set $w = R \cos \psi$, $z = -R \sin \psi$ in Eqs. (13) and (14) and take $\kappa = \delta_2 + 1/8$ which gives

$$
\begin{aligned}
\frac{dw}{dt} = -\epsilon z + \epsilon^2 \Bigg[&\left(\mu + \frac{7}{2}\right) z^3 - (\mu + 3) w z^2 + \left(\mu - \frac{3}{2}\right) w^2 z + (\kappa - 1) z - \frac{15}{8} (w^2 + z^2)^2 z \\
&- \left(\mu + \frac{1}{2}\right) w^3 \Bigg]
\end{aligned}
$$

(29)
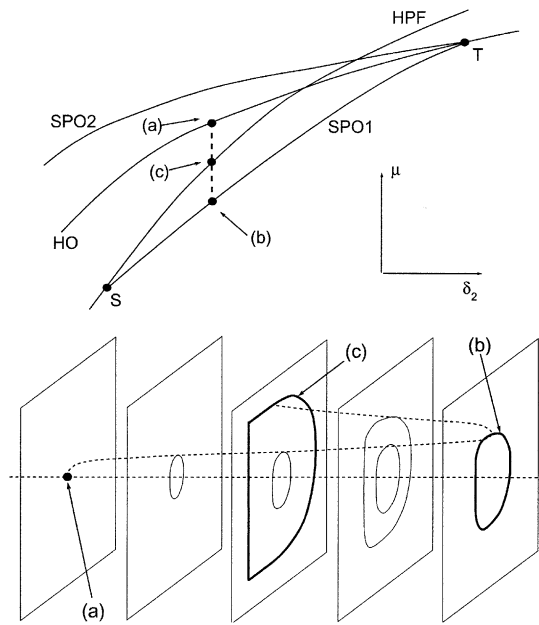
Fig. 6. Continuation procedure to obtain points on the SPO1 curve. Top shows continuation path in parameter space (dashed line). Bottom shows the evolution of the periodic orbit along the path (in polar coordinates). Point (a) corresponds to a point on the HPF curve where a Hopf bifurcation occurs, (b) is a point on the SPO1 curve and (c) is on the HO curve where a heteroclinic bifurcation occurs (straight-line segment of the heteroclinic orbit corresponds to $R = 0$). Between (b) and (c), there are two periodic orbits.
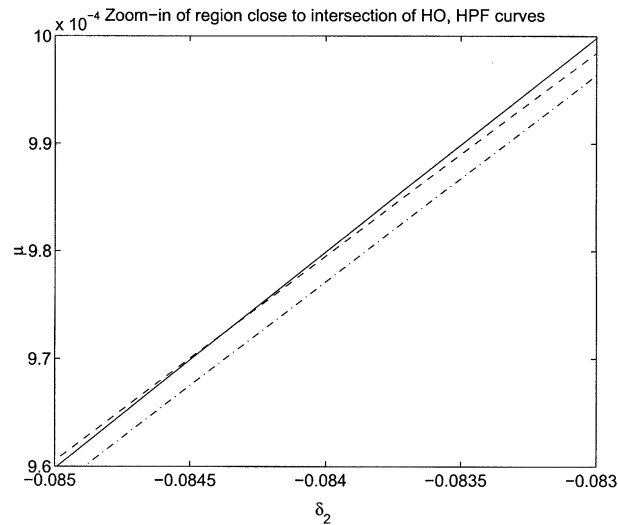
Fig. 7. Zoom-in of region close to intersection of HO, HPF cuvres. HO is dashed line. HPF is solid line. SPO1 is dashed–dotted line.
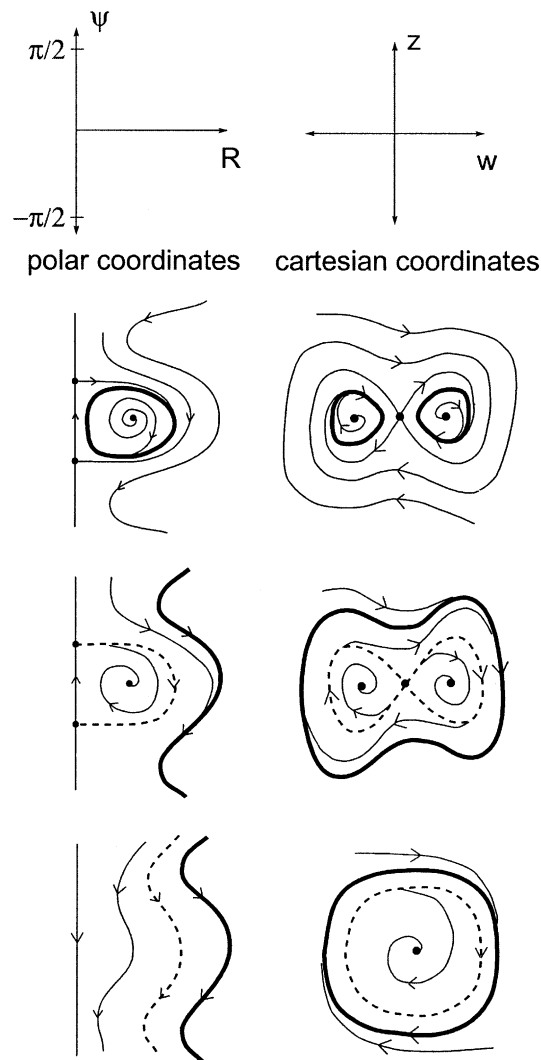
Fig. 8. Phase portraits in polar and cartesian coordinates. Darker lines correspond to stable periodic orbits. Dashed lines correspond to unstable periodic orbits.

$$\frac{\mathrm{d}z}{\mathrm{d}t} = \epsilon^2 \left[-(\mu + 1)z^3 - \left(\mu + \frac{9}{2}\right)wz^2 - \left(\mu - \frac{3}{2}\right)w^2z - \left(\mu - \frac{1}{2}\right)w^3 - \kappa w + \frac{15}{8}(w^2 + z^2)^2 w \right]$$

(30)

Obtaining an approximation for the SPO2 curve is more difficult because we cannot continue solutions from the HPF curve to the SPO2 curve. This is because in between the two curves is the heteroclinic bifurcation curve and AUTO cannot continue a periodic orbit through a heteroclinic trajectory. However, AUTO can perform continuation starting from numerical data which

specifies a periodic orbit. Thus, we can use numerical integration to obtain a starting point for AUTO to continue type 2 periodic orbits.

A numerical approximation for a type 2 limit cycle was obtained by numerically integrating Eqs. (29) and (30). To get a point on the SPO2 curve, we continue the type 2 periodic orbit decreasing δ_2 holding μ fixed. At some point AUTO will detect a fold and δ_2 will start to increase. This corresponds to a point on the SPO2 curve and if we continue after the fold, we will eventually reach the HO curve in a heteroclinic bifurcation. Fig. 9 shows an illustration of the procedure to obtain a point on the SPO2 curve.

We could have just as easily performed the same procedure holding δ_2 fixed and varying μ as long as we choose an appropriate starting point. As was done for the SPO1 curve, this procedure is repeated starting at different parameter values to obtain the SPO2 curve.

In the degenerate Hopf bifurcation, a type 2 limit cycle grows out of the origin. Although AUTO is normally able to continue Hopf bifurcation curves, the DHPF curve is degenerate and we cannot use AUTO to continue this curve directly. To see why this bifurcation is degenerate we look at the slow flow equations in cartesian coordinates. Note that if we linearize about the origin ($w = 0, z = 0$), the trace of the Jacobian is always zero. This is the condition for a non-degenerate Hopf bifurcation. We can obtain an approximation for the DHPF curve indirectly by continuing the type 2 periodic orbit down to a point where it shrinks to the origin which corresponds to the

Fig. 9. Continuation procedure to obtain points on the SPO2 curve. Top shows continuation path in parameter space (dashed line). Bottom shows the evolution of the periodic orbit along the path (in cartesian coordinates). Point (a) corresponds to the trajectory obtained from numerical integration, (b) is a point on the SPO2 curve and (c) is on the HO curve. Between (b) and (c), there are two periodic orbits.

Fig. 10. Bifurcation diagram obtained using AUTO near point Q. Bifurcation curves involving fixed points (LM1, HPF, DHF) are solid lines. HO curve is a dashed line. SPO1, SPO2 curves are dashed–dotted lines. Note, it is difficult to see the crossing of the HO and HPF curves and the SPO1 curve because they occur for a narrow band of parameter values. However, these features are distinguishable if we zoom into a region as was shown in Fig. 7.

degenerate Hopf bifurcation. In a procedure similar to those used to obtain the SPO1 and SPO2 curves, we can get an approximation for the DHPF curve.

Finally, Fig. 10 shows the completed bifurcation diagram near point Q obtained using AUTO. In Fig. 10, it is difficult to see the crossing of the HO and HPF curves and the SPO1 curve because they occur for a narrow band of parameter values. However, these features are distinguishable if we zoom into a region as was shown in Fig. 7.

7. Analytic expression for degenerate Hopf bifurcation

To obtain an expression for the degenerate Hopf bifurcation curve, we start by looking at the normal form for a Hopf bifurcation. In polar coordinates, the normal form of a Hopf bifurcation is

$$\dot{r} = (\mathrm{d}\mu + \sigma r^2 + \zeta r^4 + \cdots)r \tag{31}$$

$$\dot{\theta} = (w + c\mu + br^2 + \cdots) \tag{32}$$

When μ changes sign a limit cycle is created or destroyed at the origin and the sign of the cubic coefficient σ in the $\dot{r}$ Eq. (31) determines whether the Hopf bifurcation is supercritical or subcritical. In the non-degenerate case, $\mu = 0$ defines the curve in parameter space for a Hopf bifurcation. In our system (29) and (30), however, the trace of the Jacobian is identically zero for all parameter values. Thus $\mu = 0$ and we have a degenerate Hopf. When $\mu = 0$ Eq. (31) becomes, neglecting terms of $\mathrm{O}(r^7)$:

$$\dot{r} = (\sigma + \zeta r^2)r^3 \tag{33}$$

Now, when σ changes sign a limit cycle is created or destroyed at the origin and ζ determines if the bifurcation is supercritical or subcritical. Thus, the condition for the degenerate Hopf bifurcation is $\sigma = 0$. Guckenheimer and Holmes [3] provide a formula for this coefficient σ. For our calculations, we find it easier to use an alternative form for σ given by Perko [8] and found by Andronov for a general planar analytic system with Taylor series:

$$\dot{x} = a_{10}x + a_{01}y + a_{20}x^2 + a_{11}xy + a_{02}y^2 + a_{30}x^3 + a_{21}x^2y + a_{12}x^2y^2 + a_{03}y^3 + \cdots$$
$$\dot{y} = b_{10}x + b_{01}y + b_{20}x^2 + b_{11}xy + b_{02}y^2 + b_{30}x^3 + b_{21}x^2y + b_{12}x^2y^2 + b_{03}y^3 + \cdots \tag{34}$$

$$\begin{aligned}
\sigma = \frac{-3\pi}{2a_{01}\Delta^{3/2}} \big(& [a_{10}b_{10}(a_{11}^2 + a_{11}b_{02} + a_{02}b_{11}) + a_{10}a_{01}(b_{11}^2 + a_{20}b_{11} + a_{11}b_{02}) \\
& + b_{10}^2(a_{11}a_{02} + 2a_{02}b_{02}) - 2a_{10}b_{10}(b_{02}^2 - a_{20}a_{02}) - 2a_{10}a_{01}(a_{20}^2 - b_{20}b_{02}) \\
& - a_{01}^2(2a_{20}b_{20} + b_{11}b_{20}) + (a_{01}b_{10} - 2a_{10}^2)(b_{11}b_{02} - a_{11}a_{20})] \\
& - (a_{10}^2 + a_{01}b_{10})[3(b_{10}b_{03} - a_{01}a_{30}) + 2a_{10}(a_{21} + b_{12}) + (b_{10}a_{12} - a_{01}b_{21})] \big)
\end{aligned} \tag{35}$$

where, $\Delta = a_{10}b_{01} - a_{01}b_{10}$. In general, it is not easy to derive explicit expressions for the coefficients in the normal form. However, there are symbolic computer algebra programs which can be used to find explicit formula for the coefficients (see [10,11]).

Substituting the values for the coefficients a_{ij}, b_{ij} from Eqs. (29) and (30), we obtain an expression for the degenerate Hopf bifurcation curve DHPF. After simplifying and factoring the resulting expression we obtain:

$$2\epsilon^6\kappa(\epsilon\kappa - \epsilon - 1)(4\epsilon\kappa\mu - 2\epsilon\mu - 2\mu + 3\epsilon\kappa) = 0 \tag{36}$$

Taking the last factored term in Eq. (36), solving for μ and substituting $\kappa = \delta_2 - 1/8$ gives

$$\mu = -\frac{3\epsilon(\delta_2 - 1/8)}{4\epsilon(\delta_2 - 1/8) - 2\epsilon - 2} \tag{37}$$

Eq. (37) agrees with numerical results obtained by use of AUTO.

8. Conclusions

We have presented a complete picture of the bifurcations that occur near a degenerate bifurcation point Q for the second-order slow flow equations from a Mathieu equation with cubic nonlinearities. An analytic approximation for the heteroclinic bifurcation curve near point Q was obtained. Additional bifurcation curves for periodic orbits were also investigated numerically using AUTO. An expression for a curve of degenerate Hopf bifurcations was also obtained analytically. The second-order analysis was motivated by features observed from numerical integrations (see [6]) that first-order averaging could not explain. It is possible that going to third-order in the averaging procedure may uncover even more dynamical behavior.

Acknowledgements

References

[1] Doedel E, Champneys A, Fairgrieve T, Kuznetsov Y, Sandstede B, Wang X, et al. AUTO 97: Continuation and Bifurcation Software for Ordinary Differential Equations 1998.
[2] El-dib YO. Nonlinear Mathieu equation and coupled resonance mechanism. Chaos Solitons Fract 2001;12(4):705–20.
[3] Guckenheimer J, Holmes P. Nonlinear Oscillators Dynamical Systems and Bifurcations of Vector Fields. New York: Springer-Verlag; 1983.
[4] Kidachi H, Onogi H. Note on the stability of the nonlinear Mathieu equation. Prog Theor Phys 1997;98(4):755–73.
[5] Norris J. The nonlinear Mathieu equation. Int J Bifurcation Chaos 1994;4(1):71–86.
[6] Ng L, Rand R. Bifurcations in a Mathieu equation with cubic nonlinearities. Chaos Solitons Fract 2002;14(2):173–81.
[7] Ng L. Ph.D. thesis, Cornell University, New York, 2002.
[8] Perko L. Differential equations and dynamical systems. New York: Springer-Verlag; 1996.
[9] Rand RH. Topics in nonlinear dynamics with computer algebra. New York: Gordon and Breach; 1994.
[10] Rand RH, Armbruster D. Perturbation methods, bifurcation theory and computer algebra. Boston: Pitman; 1984.
[11] Yu P. Computation of normal forms via a perturbation technique. J Sound Vibr 1998;211:19–38.